The Transition From Weak to Strong Diffuse Radar Bistatic Scattering From Rough Ocean Surface

Alexander G. Voronovich and Valery U. Zavorotny, *Fellow, IEEE*

***Abstract*— Many of the currently used models of scattering from a rough ocean surface are designed for the regime of strong diffuse scattering that takes place at large Rayleigh parameter R_a. Using them for the case of weak, or even moderate diffuse scattering that is characterized by $R_a \lesssim 1$ would lead to an incorrect result. At the same time, for practical applications, it is important to describe the transition from partially coherent scattering to completely noncoherent, strong diffuse scattering in terms of the bistatic radar cross section σ_0. This situation may occur for scattering of global navigation satellite system (GNSS) signals or other signals of opportunity from a rough ocean surface under weak winds, or from ice. In this paper, we obtain an expression for σ_0 for the case of weak-to-moderate diffuse scattering using a formulation based on the small slope approximation of the first order. For a reasonable range of R_a, calculations can be quickly performed using standard desktop computers. We demonstrate results of such calculations for bistatic radar scattering for L-band at low-to-moderate R_a and its transition to σ_0 at large values of R_a.**

***Index Terms*— Radar cross section, radar scattering, rough surfaces, sea surface electromagnetic scattering.**

I. Introduction

PHASE variations of ocean scattered radio waves can be quantified by the Rayleigh roughness parameter R_a which is proportional to a ratio of the surface standard deviation to the radio wavelength, times the cosine of the angle of incidence (see [1]). Most of the currently used bistatic scattering models from rough ocean surface are designed for the regime of strong diffuse scattering that takes place at a large Rayleigh parameter R_a (see [2], [3]). However, in the case of scattering from a slightly rough ocean surface (generated by weak winds) or scattering from ice, the Rayleigh parameter could be moderate or even small [4]. In such situations, models based on a large Rayleigh parameter assumption will lead to incorrect results. In the case of very small values of R_a, the rough surface scattering will be dominated by a coherent, specular reflection component which is absent in the case of a large Rayleigh parameter. When the value of R_a grows, the coherent specular component quickly decays giving way to noncoherent diffuse scattering.

For practical applications of bistatic radar scattering from the ocean surface (see [4]–[8]), it is important to understand how the transition from partially coherent scattering to completely noncoherent, strong diffuse scattering takes place and to be able to model such a scattering regime for arbitrary values of the Rayleigh parameter including the cases of small and moderate R_a. In the general case, the power of the coherent component is proportional to the power of the signal produced by a mirror image of the source (or the receiver) multiplied by the square of the average reflection coefficient $|\overline{V}|^2$. At the same time, the power of the diffuse component is proportional to the surface integral associated with the noncoherent bistatic radar cross section (BRCS) σ_0.

In Section II, we obtain expressions for both $|\overline{V}|^2$ and σ_0 using a formulation based on the small slope approximation of the first order (SSA1) which is used for electromagnetic wave scattering calculations for a variety of rough surfaces, from ocean to land (see [3], [9]). Here, we consider a specific case of the ocean surface with roughness obeying Gaussian statistics; this statistics can be fully described by the correlation function of surface heights. In Section III, following the perturbative approach, the exponential under the SSA1 surface integral can be approximated by a polynomial with a finite number of terms. As a result, the expression for σ_0 becomes a finite sum of terms, and each of which contains a Fourier transform of the surface correlation function raised to a power equal to the index of the corresponding term of the sum. The larger the R_a is, the larger the number of terms that needs to be accounted for in order to have a converging result. Such a Fourier transform being proportional to the multiple convolution of the roughness spectrum is always a positive value. The coefficients of the polynomial expansion are also positive. Therefore, summation does not lead to what is known in numerical computations as the effect of catastrophic cancellation, or loss of significance. For a reasonable range of R_a, calculations of such sums can be quickly performed using standard desktop computers.

A similar expansion based on the integral equation method (IEM) was used in [10] and [11] for simulations of incoherent bistatic scattering from the sea surface. The SSA1 method used here is more advantageous since it is more accurate in calculating scattering at wider scattering angles (see a discussion of this issue in [12]).

This paper complements our previous work [3] that was devoted to the SSA method applied to the opposite case of strong diffuse scattering. Section IV demonstrates results of σ_0 calculations for the circular polarization at L-band which is typical for the global navigation satellite system (GNSS) reflectometry applications. We analyze a transition of σ_0 from the low-to-moderate R_a, to large values of R_a in the course of which we observe a bimodal behavior in the angular dependence of $\sigma_0(\vec{k}, \vec{k}_0)$.

Manuscript received April 17, 2017; revised August 8, 2017; accepted August 28, 2017. Date of publication September 14, 2017; date of current version October 27, 2017. *(Corresponding author: Valery U. Zavorotny.)*

The authors are with the Earth System Research Laboratory, National Oceanic and Atmospheric Administration, Boulder, CO 80305 USA (e-mail: alexander.voronovich@noaa.gov; valery.zavorotny@noaa.gov).

Digital Object Identifier 10.1109/TAP.2017.2752219

II. Problem Formulation

The process of electromagnetic wave scattering from the rough ocean surface can be conveniently described in terms of a scattering amplitude as a function of horizontal components of wave vectors, for incident and scattered plane waves (see [13]). Let the wave vector of the incident plane wave be $\vec{K}_0 = (\vec{k}_0, -q_{k_0})$, where $\vec{k}_0$ and q_{k_0} are, respectively, its horizontal projection of the wave vector and the vertical wavenumber. Note that $q_{k_0} = (\omega^2/c^2 - k_0^2)^{1/2}$. Similarly, for the wave vector of the scattered plane wave, one has $\vec{K} = (\vec{k}, q_k)$. Using the scattering amplitude approach, the angular distribution of the average power of the scattered signal can be expressed via the generalized scattering cross section $\mathcal{E}$ which includes both coherent and noncoherent (diffuse) components [13]

$$\mathcal{E}(\vec{k}, \vec{k}_0) = |\overline{V}(\vec{k})|^2 \delta(\vec{k} - \vec{k}_0) + \frac{1}{4\pi\, q_k q_{k_0}} \sigma_0(\vec{k}, \vec{k}_0) \tag{1}$$

where $\overline{V}(\vec{k})$ is the average reflection coefficient and $\sigma_0(\vec{k}, \vec{k}_0)$ is the diffuse scattering cross section per unit area. Therefore, for calculation of the first- and second-order statistical moments of a scattered field in the far zone, it is sufficient to know two parameters: average reflection coefficient $\overline{V}(\vec{k})$ and scattering cross section $\sigma_0(\vec{k}, \vec{k}_0)$. In the case of the first statistical moment of the scattered field (i.e., the average field), scattering reduces to reflection in the specular direction. For this reason, $\vec{k} = \vec{k}_0$, and the average reflection coefficient $\overline{V}$ depends on a single argument. The power of the coherent component is proportional to the power of the signal produced by a mirror image of the source multiplied by the square of the average reflection coefficient $|\overline{V}|^2$. On the other hand, the scattering cross section σ_0 describes a noncoherent, diffuse scattering that is governed by the second statistical moment of the fluctuations of the scattered field from which the average field was subtracted.

Average reflection coefficient and scattering cross section can only be calculated theoretically approximately. The most widely used theoretical approaches are the small perturbation method and the Kirchhoff (tangent plane) approximation which are applicable for the cases of small R_a and for smooth surfaces, respectively. A more general unifying approach is provided, in particular, by the SSA [13], which is applicable to the roughness with small slopes regardless of the value of the Rayleigh parameter. In this paper, we will be using the SSA1.

The general expression for the average reflection coefficient $\overline{V}(\vec{k})$ in the case of Gaussian statistics of elevations h reads [13]

$$\overline{V}(\vec{k}) = e^{-2q_k^2\langle h^2\rangle}\left[V_F(\vec{k}) + 2q_k^2\langle h^2\rangle V_F(\vec{k})\right] + e^{-2q_k^2\langle h^2\rangle} q_k \int B_2(\vec{k}, \vec{k}; \vec{k} + \vec{\xi})\, \widehat{W}(\vec{\xi})\, d\vec{\xi}. \tag{2}$$

Here, $V_F(\vec{k})$ is the Fresnel reflection coefficient, $\widehat{W}(\vec{\xi})$ is the surface roughness spectrum with the standard normalization

$$\langle h^2\rangle = \int \widehat{W}(\vec{\xi})\, d\vec{\xi} \tag{3}$$

and B_2 is a nonsingular function that depends on a type of the field and boundary conditions. The explicit expression for B_2 for the case of electromagnetic waves can be found in [14]. One can see that for large values of the Rayleigh parameter

$$R_a = q_k \langle h^2\rangle^{1/2}. \tag{4}$$

$\overline{V}(\vec{k})$ is exponentially small, and the effects of the average field can be neglected. For small and moderate R_a, the main dependence of $\overline{V}$ on R_a is still in the exponential factor in (2), and in the first approximation, the correction terms in the parenthesis, which are of the order of the square of slopes, can be neglected. Then, one obtains

$$\overline{V}(\vec{k}) \approx e^{-2R_a^2} V_F(\vec{k}). \tag{5}$$

This result also follows from the Kirchhoff approximation (see [1], [13]), which is natural because both methods produce the same expressions for a scattered field in the specular direction. We suggest using (5) as far as calculation of $\overline{V}(\vec{k})$ is concerned.

The expression for the dimensionless diffuse scattering cross section in the SSA1 reads [13]

$$\sigma_0(\vec{k}, \vec{k}_0) = |B(\vec{k}, \vec{k}_0)|^2 \frac{4q_k^2 q_{k_0}^2}{\pi (q_k + q_{k_0})^2} \times e^{-(q_k + q_{k_0})^2 W(0)} \int e^{-i(\vec{k} - \vec{k}_0)\vec{\rho}} \times (e^{(q_k + q_{k_0})^2 W(\vec{\rho})} - 1) d\vec{\rho}. \tag{6}$$

Here, $W(\vec{\rho})$ is the correlation function of the surface roughness

$$W(\vec{\rho}) = \langle h(\vec{r}) h(\vec{r} + \vec{\rho})\rangle = \int e^{i\vec{\xi}\vec{\rho}}\, \widehat{W}(\vec{\xi}) d\vec{\xi}. \tag{7}$$

When only vertically polarized electromagnetic waves are transmitted and received after being scattered, the expression for B reads

$$B(\vec{k}, \vec{k}_0) = \frac{(\varepsilon - 1)(q_k^{(\varepsilon)} q_{k_0}^{(\varepsilon)} \frac{\vec{k}\vec{k}_0}{k k_0} - \varepsilon k k_0)}{(\varepsilon q_k + q_k^{(\varepsilon)})(\varepsilon q_{k_0} + q_{k_0}^{(\varepsilon)})} \tag{8}$$

where ε is a complex dielectric constant of the sea water ($\mathrm{Im}(\varepsilon) \geq 0$); $q_k^{(\varepsilon)} = (\varepsilon\omega^2/c^2 - k^2)^{1/2}$ is the vertical component of the wave vector in the sea water ($\mathrm{Im}\, q_k^{(\varepsilon)} > 0$). Formulae for B for other polarizations can be found in [14].

The expression (6) contains the same integral as the expression for σ_0 obtained with the Kirchhoff approximation; the preintegral factor is, however, different (see [12], [13]). The most important difference between the Kirchhoff approximation and the SSA1 is that the correlation function $W(\vec{\rho})$ in (6) is not generally assumed to be slowly varying (on the scale of wavelength) and may contain small-scale components responsible for Bragg scattering. The discussion of a superior accuracy of the SSA compared to the Kirchhoff approximation and discrepancies between them can be found in [3] and [12]–[14].

In the case of a large Rayleigh parameter, and if the Bragg scattering can be neglected, the scattering will be due to the tilted facets of large-scale roughness, and it proceeds in the

narrow cone around the nominal specular direction. Then, one can set in (6)

$$\frac{4q_k^2 q_{k_0}^2}{(q_k+q_{k_0})^2} \approx q_k^2 \tag{9}$$

and make use of the following approximation:

$$|B(\vec{k},\vec{k}_0)|^2 \approx |B(\vec{k},\vec{k})|^2. \tag{10}$$

Since scattering is concentrated in the vicinity of the specular direction, it does not matter if either $\vec{k}$ or $\vec{k}_0$ is substituted in the right-hand sides of (9) and (10). It can be proven [13] that in the general case the following relation holds:

$$V_F(\vec{k}) = B(\vec{k},\vec{k}). \tag{11}$$

One can additionally expand $W(\vec{\rho})$ in the exponent of the integrand of (6) into a power series keeping the two first terms. In this case, SSA1 essentially reduces to the geometrical optics approximation. The resulting Gaussian integral is easily calculated, providing an explicit expression for $\sigma_0(\vec{k},\vec{k}_0)$ identical to that obtained in [2].

In the opposite limiting case of small R_a, (6) reduces to the standard expression for the scattering cross section in the small perturbation method [15]. However, for our purposes, this approximation is not sufficient because we will be considering the case of small-to-moderate values of the Rayleigh parameter. To this effect, we will compute the integral in (6) using the procedure described in the next section.

Thus, in the case of a small R_a, rough surface acts more like a mirror, only slightly degrading the coherence of a reflected wave. Still, a weak diffuse scattering simultaneously exists at nonspecular directions. When the value of R_a grows, the weakly diffuse scattered field becomes increasingly stronger, whereas the coherent specular component quickly decays. In what follows, we will assume that the values of R_a are small or moderate. It is important to understand the details of the transition from partially coherent scattering to completely noncoherent, diffuse scattering. This will be done in the following section.

III. Numerical Implementation

The calculation of the specular component of the scattered signal given by (5) is straightforward, so our focus will be on the calculation of the diffuse scattering cross section $\sigma_0(\vec{k},\vec{k}_0)$. For practical applications, when σ_0 needs to be estimated for a large array of $\vec{k},\vec{k}_0$, one has to be able to evaluate $\sigma_0(\vec{k},\vec{k}_0)$ fast enough. Since the integral in (6) is a two-dimensional Fourier transform, it can be calculated using the fast fourier transform (FFT). However, a direct application of the FFT is not practical, since the exponent in (6) depends on incidence and scattering angles through $(q_k+q_{k_0})$, and one has to apply a 2-D FFT anew for every combination of these angles, which will be too time-consuming for the calculation of waveforms. To bypass this difficulty, we may take into account that for moderate values of the Rayleigh parameter the exponential in (6) can be approximated by a polynomial with a finite number of terms

$$e^{(q_k+q_{k_0})^2 W(\vec{\rho})} - 1 \approx \sum_{l=1}^{L} \frac{(q_k+q_{k_0})^{2l}}{l!} W^l(\vec{\rho}). \tag{12}$$

Let us introduce the following notation:

$$\widehat{W}^{(l)}(\vec{\xi}) = \int e^{-i\vec{\xi}\vec{\rho}} W^l(\vec{\rho}) \frac{d\vec{\rho}}{(2\pi)^2}. \tag{13}$$

For $l = 1$, (13) reduces to the expression for standard roughness spectrum used in (3) and (7)

$$\widehat{W}^{(1)}(\vec{\xi}) = \widehat{W}(\vec{\xi}). \tag{14}$$

Now (6) becomes

$$\sigma_0(\vec{k},\vec{k}_0) = 16\pi q_k^2 q_{k_0}^2 |B(\vec{k},\vec{k}_0)|^2 \times e^{-(q_k+q_{k_0})^2 W(0)} \sum_{l=1}^{L} \frac{(q_k+q_{k_0})^{2l-2}}{l!} \widehat{W}^{(l)}(\vec{k}-\vec{k}_0). \tag{15}$$

To calculate $\widehat{W}^{(l)}(\vec{\xi})$, one applies the FFT for each l only once; the dependence of $\sigma_0(\vec{k},\vec{k}_0)$ on incidence/scattering angles in (15) is now contained only in simple factors. Thus, the calculation of $\sigma_0(\vec{k},\vec{k}_0)$ according to (15) for not too large L is feasible on modern desktop computers.

It is important to emphasize that the right-hand side of (13) being expressed in terms of a standard roughness spectrum $\widehat{W}(\vec{\xi})$ represents multiple convolutions of the roughness spectrum which is a non-negative function. For this reason, all factors $\widehat{W}^{(l)}(\vec{\xi})$ are non-negative. The coefficients in front of $\widehat{W}^{(l)}(\vec{k}-\vec{k}_0)$ in the sum in (15) are also positive. For this reason, the catastrophic cancellation of terms in the sum in (15) does not take place. In the numerical simulations performed for the case of L-band signals, results of which are shown in the next section, we summed up to $L \sim 150$ terms. The number of series terms L is different for each case of incidence angle and wind speed, and it is determined by the value of the Rayleigh parameter: the larger the Rayleigh parameter is, the larger the number L that should be used. The calculation of the next term in the series continues until the value of this term becomes less than a certain share of the total sum (in our case, less than 1%).

We should mention here that an expansion similar to (12) was used in [10] and [11] for simulations of incoherent bistatic scattering from the sea surface at L-band using the IEM. The IEM expression for σ_0 used in [10] and [11] is similar to (15); however, the polarization-dependent coefficient analogous to $|B(\vec{k},\vec{k}_0)|^2$ has a somewhat different form. Those simulations were concerned with strong diffuse scattering, so the number of terms L was so large that it required the use of supercomputers. Note that the numerical implementation of the SSA method developed in [3] for the case of strong diffuse scattering does not require such summation, and the computation time remains reasonably short even with standard desktop computers.

IV. Numerical Results

Having in mind GNSS reflectometry applications [6], [7], all calculations below were performed assuming that the incident field is of right-hand circular polarization and the received field is of left-hand circular polarization. In this case, coefficient B above can be expressed as a corresponding linear combination

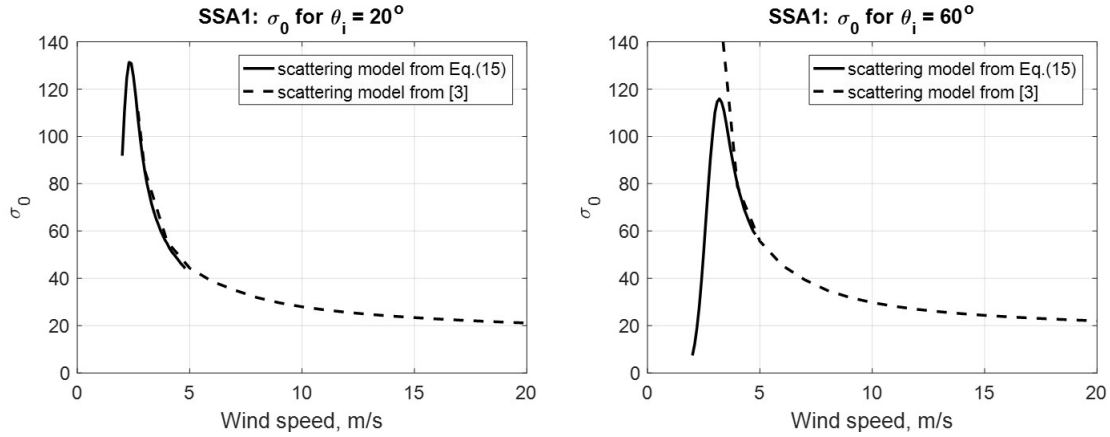

Fig. 1. BRCS in a specular direction as a function of wind speed from 2 to 20 m/s for incidence angles 20° (left) and 60° (right). The incidence plane is aligned with the wind direction, although for the specular direction it does not matter because for this case the BRCS is not sensitive to the wind direction.

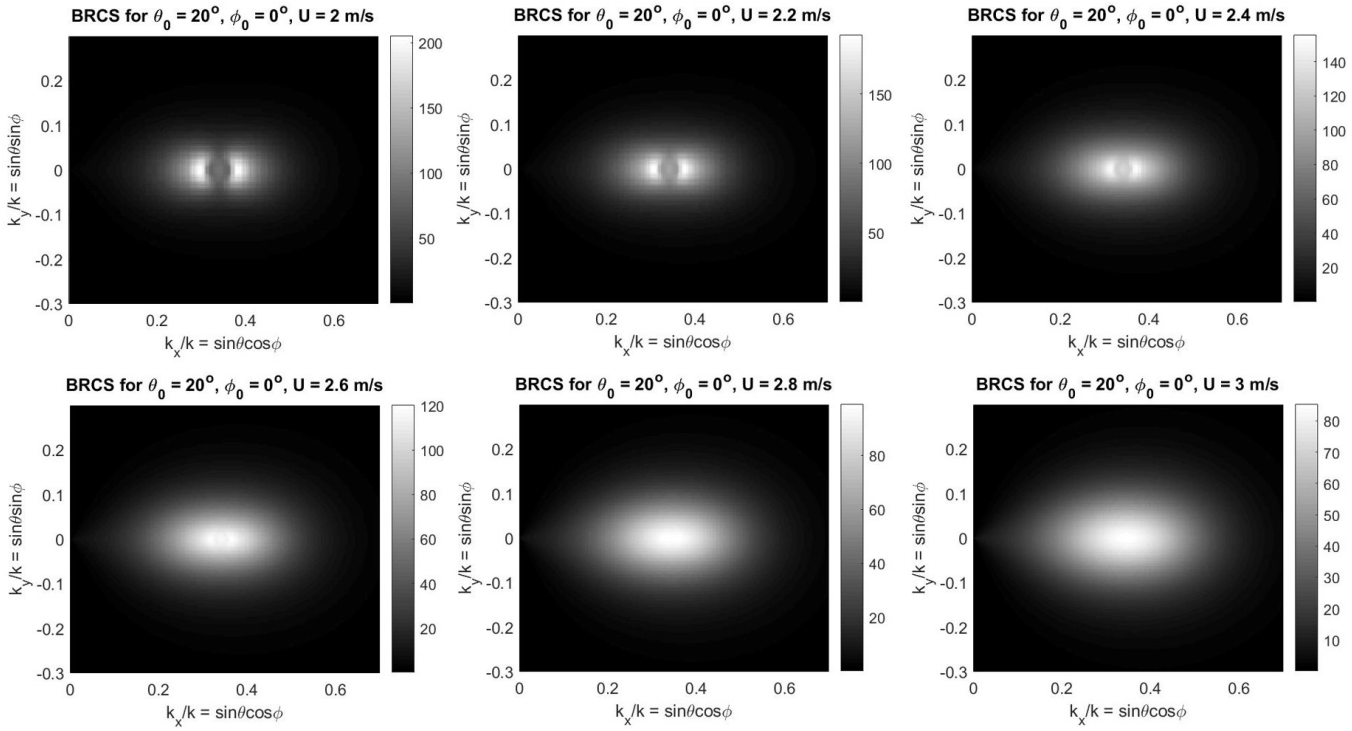

Fig. 2. BRCS as a function of the scattering angle for the range of low wind speeds from 2 to 3 m/s. The incidence angle is 20°, and the incidence plane is aligned with the wind direction.

of $B_{\alpha\beta}(\vec{k}, \vec{k}_0)$ functions from [14] (here $\alpha, \beta = 1, 2 \equiv V, H$). The frequency was set to $f = \omega/2\pi = 1.57$ GHz and the Elfouhaily *et al.* spectrum [16] was used for $\widehat{W}(\vec{\xi})$.

Fig. 1 shows the results of calculations of the bistatic scattering cross section $\sigma_0(\vec{k}_0, \vec{k}_0)$ in a specular direction as a function of wind speed for incidence angles 20° (the left plot) and 60° (the right plot). The incidence plane is aligned with the wind direction, although for the specular direction it does not matter because for this case the σ_0 is not sensitive to the wind direction. The complex dielectric constant ε of sea water and for L-band EM waves was chosen $74.44 + i49.88$. We calculated σ_0 for an overlapping interval of winds using both expression (15) and the method presented in [3] for the case $R_a \gg 1$ to show the difference between them and to find out where the results of both methods are merging. For incidence angles between 20° and 60°, the merger interval of winds is between $U = 3$ m/s and $U = 5$ m/s. This corresponds to the interval of R_a between 13 and 100 for the incidence angle of 20°, and to the interval of R_a between 4 and 28 for the incidence angle of 60°. The dashed curves are related to wind speed larger than 3 m/s. They are obtained with the algorithm presented in [3]. The solid curves are related to wind speed below 5 m/s, and represent the results of calculations made according to (15). For the left plot, from $L = 7$ to $L = 150$ terms were used in the expansion (15), while R_a was changing from 2.4 to 100, respectively. For the

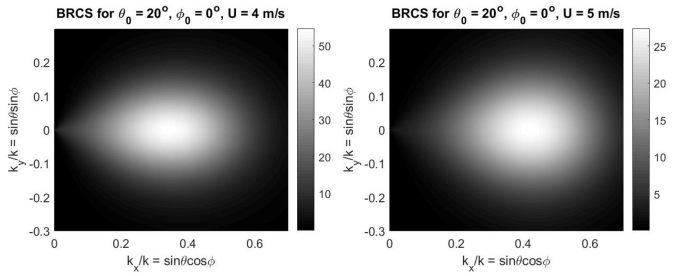

Fig. 3. BRCS as a function of scattering angles for moderate wind speeds 4 and 5 m/s. The incidence angle is 20°, and the incidence plane is aligned with the wind direction.

right plot, the range of L was from 4 to 39, with R_a changing from 0.7 to 28, respectively. The plots demonstrate a smooth transition between the results obtained by two approaches: one is more suitable for the low-to-moderate R_a, and the other is applicable only for large values of R_a.

In Fig. 2, one can see the bistatic scattering cross section $\sigma_0(\vec{k}, \vec{k}_0)$ represented as a 2-D function of scattering angles for a range of low wind speeds from 2 to 3 m/s. The incidence angle is 20°, and the incidence plane is aligned with the wind direction. Calculations were made according to (15) and the format of the map follows [9], where $k_x/k = \sin\theta\cos\phi$ and $k_y/k = \sin\theta\sin\phi$. One can see that there is a depression in the diffuse scattering diagram in the specular direction surrounded by two distinct peaks in the plane of incidence ($k_y/k = 0$) for 2 to 2.4 m/s wind speeds. Note that for this particular incidence angle of 20°, this bimodality disappears for larger R_a, namely, for winds 2.6 m/s and stronger. This phenomenon is due to the behavior of the sea wave spectrum at the low-frequency end which goes to zero for sufficiently long waves [16]. Indeed, for the specular direction, we have $\vec{k} = \vec{k}_0$, and the first term in the sum of (15) representing first-order Bragg scattering goes to zero since for the sea wave spectrum $\widehat{W}(0) = \widehat{W}^{(1)}(0) = 0$. With the wind increase, the higher order terms in (15) $\widehat{W}^{(l)}$, $l = 2, 3, \ldots$ for which $\widehat{W}^{(l)}(0) > 0$ start to contribute and the dip in the specular direction gradually fills in. This is illustrated in the second row of the plots in Fig. 2 which demonstrates a unimodal scattering lobe with a gradually decreasing peak value for moderate winds shown in Fig. 3.

The bimodal phenomenon is illustrated more clearly by Fig. 4 which shows the 1-D cuts of the scattering cross-sectional diagram along the scattering angle for the case of 45° incidence angle for the same range of weak winds. (Both incident and scattered waves are aligned in the azimuthal direction with the wind direction, i.e., $\phi = 0$). One can see that the behavior of σ_0 in the specular direction is not monotonic in this range of wind speed values. It peaks at wind speed 2.4–2.6 m/s, although the exact position of this peak depends on the incidence angle value. Therefore, the diffuse bistatic cross section σ_0 taken in the specular direction does not grow limitlessly when wind speed goes to zero as the SSA1 model for strong diffuse scattering predicts [3]. From the physical point of view, this behavior of σ_0 is understandable; surface roughness disappears when the wind dies out, so the reason for diffuse scattering vanishes as well. At the same time, when surface roughness is getting weaker and weaker ($R_a \ll 1$) the

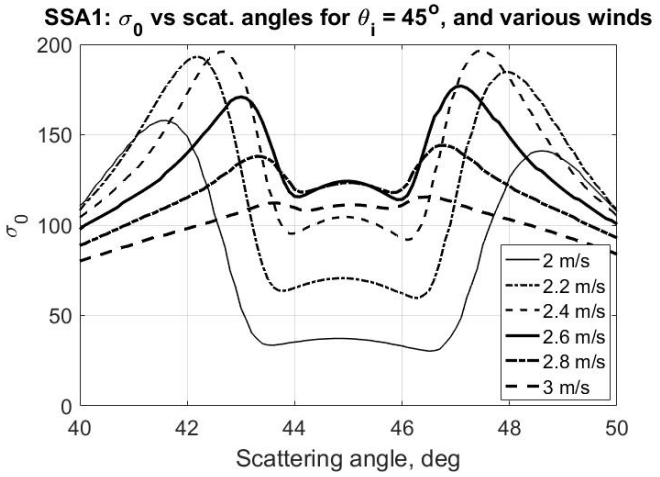

Fig. 4. BRCS at $\phi = 0$ as a function of the zenith scattering angle θ for the range of low wind speeds from 2 to 3 m/s. The incidence angle is 45°, and the incidence plane is aligned with the wind direction.

average reflection coefficient grows according to (5). Thus, with decreasing wind, the reflected signal in the specular direction will be eventually dominated by the coherent component.

Calculations of 2-D maps of $\sigma_0(k_x/k, k_y/k)$ for other values of incidence zenith and azimuth angles demonstrate similar behavior over the k_x/k, k_y/k plane with corresponding shifts of the σ_0 maximum position.

V. Conclusion

The previously suggested model for waveform calculations for scattering from a rough ocean surface [2] was designed for the regime of strong diffuse scattering, i.e., for the large Rayleigh parameter $R_a \gg 1$. Using it for the case of weak, or even moderate diffuse scattering $R_a \lesssim 1$ would lead to an incorrect result. Here, we developed a model for the BRCS $\sigma_0(\vec{k}, \vec{k}_0)$ for the case of weak-to-moderate diffuse scattering based on the SSA1 which provides a smooth transition from weak through moderate into the strong diffuse scattering regime. However, the calculation of σ_0 with the presented method for the regime of strong diffuse scattering requires a very large number L of series terms which is proportional to the Rayleigh parameter used, so it becomes prohibitively slow. In this case, the use of the approach developed in [3] is more advisable.

This model can be used to calculate delay-Doppler maps for the purposes of GNSS reflectometry of the sea surface in the case of low winds. Other relevant scattering scenario might include lakes, relatively flat land, or sea ice characterized by small R_a.

References

[1] F. T. Ulaby and D. G. Long, "Microwave radar and radiometric remote sensing," Univ. Michigan Press, Ann Arbor, MI, USA, 2014, p. 427. [Online]. Available: http://mrs.eecs.umich.edu/about_authors/about_authors.html

[2] V. U. Zavorotny and A. G. Voronovich, "Scattering of GPS signals from the ocean with wind remote sensing application," *IEEE Trans. Geosci. Remote Sens.*, vol. 38, no. 2, pp. 951–964, Mar. 2000.

[3] A. G. Voronovich and V. U. Zavorotny, "Full-polarization modeling of monostatic and bistatic radar scattering from a rough sea surface," *IEEE Trans. Antennas Propag.*, vol. 62, no. 3, pp. 1362–1371, Mar. 2014.
[4] A. Alonso-Arroyo, V. U. Zavorotny, and A. Camps, "Sea ice detection using U.K. TDS-1 GNSS-R data," *IEEE Trans. Geosci. Remote Sens.*, vol. 55, no. 9, pp. 4989–5001, Sep. 2017.
[5] S. Gleason *et al.*, "Detection and Processing of bistatically reflected GPS signals from low Earth orbit for the purpose of ocean remote sensing," *IEEE Trans. Geosci. Remote Sens.*, vol. 43, no. 6, pp. 1229–1241, Jun. 2005.
[6] S. Gleason, S. Lowe, and V. Zavorotny, "Remote sensing with bistatic GNSS reflections," in *GNSS Applications and Methods*, S. Gleason and D. Gebre-Egziabher, Eds. Boston, MA, USA: Artech House, 2009, pp. 399–436.
[7] V. U. Zavorotny, S. Gleason, E. Cardellach, and A. Camps, "Tutorial on remote sensing using GNSS bistatic radar of opportunity," *IEEE Geosci. Remote Sens. Mag.*, vol. 2, no. 4, pp. 8–45, Dec. 2014.
[8] C. S. Ruf *et al.*, "New ocean winds satellite mission to probe hurricanes and tropical convection," *Bull. Amer. Meteorol. Soc.*, vol. 97, no. 3, pp. 385–395, 2016.
[9] J. T. Johnson and J. D. Ouellette, "Polarization features in bistatic scattering from rough surfaces," *IEEE Trans. Geosci. Remote Sens.*, vol. 52, no. 3, pp. 1616–1626, Mar. 2014.
[10] A. K. Fung, C. Zuffada, and C. Y. Hsieh, "Incoherent bistatic scattering from the sea surface at L-band," *IEEE Trans. Geosci. Remote Sens.*, vol. 39, no. 5, pp. 1006–1012, May 2001.
[11] C. Zuffada, A. Fung, J. Parker, M. Okolicanyi, and E. Huang, "Polarization properties of the GPS signal scattered off a wind-driven ocean," *IEEE Trans. Antennas Propag.*, vol. 52, no. 1, pp. 172–188, Jan. 2004.
[12] T. Elfouhaily and C. A. Guérin, "A critical survey of approximate scattering wave theories from random rough surfaces," *Waves Random Media*, vol. 14, no. 4, pp. R1–R40, 2004.
[13] A. G. Voronovich, *Wave Scattering From Rough Surfaces*, 2nd ed. Berlin, Germany: Springer, 1999.
[14] A. G. Voronovich and V. U. Zavorotny, "Theoretical model for scattering of radar signals in K_u- and C-bands from a rough sea surface with breaking waves," *Waves Random Media*, vol. 11, no. 3, pp. 247–269, 2001.
[15] D. E. Barrick, "First-order theory and analysis of MF/HF/VHF scatter from the sea," *IEEE Trans. Antennas Propag.*, vol. AP-20, no. 1, pp. 2–10, Jan. 1972.
[16] T. Elfouhaily, B. Chapron, K. Katsaros, and D. Vandemark, "A unified directional spectrum for long and short wind-driven waves," *J. Geophys. Res.*, vol. 102, no. C7, pp. 15781–15796, 1997.

Alexander G. Voronovich received the M.Sc. degree in physics and the Ph.D. degree in theoretical and mathematical physics from the Moscow Institute of Physics and Technology, Moscow, Russia, in 1972 and 1975, respectively, and the Dr.Sc. degree in theoretical and mathematical physics from the Acoustical Institute, Moscow, in 1988.

From 1975 to 1979, he was a Junior Research Scientist with the Acoustical Institute. In 1980, he joined the P. P. Shirshov Institute of Oceanology, Moscow, as a Senior Research Scientist. From 1989 to 1993, he was the Head of the Laboratory of Acoustical Waves Propagation in the Ocean at the P. P. Shirshov Institute of Oceanology. He then became a Professor of physics with the Moscow Institute of Physics and Technology in 1991. He is currently an Oceanographer with the Earth System Research Laboratory, National Oceanic and Atmospheric Administration, Boulder, CO, USA. His current research interests include wave scattering from rough surfaces, ocean acoustics, geophysical hydrodynamics, internal waves, and linear and nonlinear theory of wave propagation.

Dr. Voronovich is a fellow of the Acoustical Society of America.

Valery U. Zavorotny (M'01–SM'03–F'10) received the M.Sc. degree in radio physics from Gorky State University, Gorky, Russia, in 1971, and the Ph.D. degree in physics and mathematics from the Institute of Atmospheric Physics, USSR Academy of Sciences, Moscow, Russia, in 1979.

From 1971 to 1990, he was with the Institute of Atmospheric Physics, USSR Academy of Sciences. In 1990, he joined the Lebedev Physical Institute, Moscow. He is currently a Physicist with the Earth System Research Laboratory, National Oceanic and Atmospheric Administration, Boulder, CO, USA. He is also a member of the NASA CYGNSS Mission Science Team. His current research interests include the theory of wave scattering from rough surfaces, ocean, and land remote sensing applications using radar, and global navigation satellite system reflection techniques.

Dr. Zavorotny is a member of the American Geophysical Union and Commission F of the U.S. National Committee of URSI. He was a recipient of the 2014 Prince Sultan Bin Abdulaziz International Creativity Prize for Water (jointly with K. Larson, E. Small, and J. Braun). He is a Distinguished Lecturer of the Geoscience and Remote Sensing Society.